A heavy-duty magnetorheological fluid mount with flow and squeeze model

Jincheng Huang, Shaoqi Li, Yuxian Zhou, Tiancheng Xu, Yancheng Li, Huixing Wang and Shuguang Wang

Abstract

In this paper, a new type of heavy-duty magnetorheological fluid (MRF) mount is proposed and experimentally investigated. The MRF mount with both annular and radial channels are based on two operating modes: flow mode and squeeze mode. The combined paths can lengthen the MRF valve and hence maximize the MR effect in flow mode. A mechanical model is established to institutively predict the maximum damping force that the device can achieve. Magnetic field distribution of the MRF mount is then evaluated based on finite element analysis. Both squeeze and flow regions can obtain magnetic field intensities up to 0.742 T and 0.7 T under 1A current, respectively. Finally, the quasi-static and dynamic tests of MRF mount under different loading conditions (frequency, amplitude, current) are performed and the results showed that the proposed MRF mount can provide large damping force up to 18.843 kN and wide tunable range (719% increase on damping force at 0.1 Hz with 2mm amplitude).

Keywords: MRF mount; MR fluid; Heavy duty; Damping force

1. Introduction

MRF is an intelligent material with the capability to change its rheological properties in milliseconds when exposed to an external magnetic field [1-3], and the process of dramatic rheological change is called MR effect. Using this remarkable feature, many

applications have been proposed, such as automotive semi-active suspension system [4, 5], engine mount system, seismic protection systems of bridges and buildings [6-10].

MRF mount is a type of intelligent devices with the ability to generate controllable force in the vertical direction. With such capability, it can offer superior effectiveness in vibration absorption/isolation when facing the unpredictable external excitation compared with passive vibration mount. The merits to evaluate the capabilities of the MRF mount are adaptive range, maximum force output, overall compactness and power consumption, in which many of them are cross-correlated. For example, typically, to have a large force output, it requires large current applied or large dimension which inevitably leads to high energy consumption, defeating the true essence of semi-active control since low energy requirement is preferable. Alternatively, MR fluids with high zero-field viscosity can be used for large force output but it compromises the MR effect. Table 1 summaries the above parameters in the MRF mount designs available in the open literatures. These designs with large force output usually have either low force increase or high power consumption.

There are significant demands in designing a vibration mount with large force output and distinctive adaptive range within confined configuration. Typically, examples are the cases where heavy payloads are present such as floor vibration control [11, 12], vibration isolation of heavy-duty machine [13, 14], and vibration control of vehicle suspension [15]. As seen in Table 1, there is a dilemma between large force output and high adaptive range, i.e., MRF mount with large force capacity has low adaptive range, and vice versa. There is need to accomplish both in a design while

maintains low power consumption. To address this, comprehensive design process is to consider and the selection of the operation mode(s) is the first step.

There are three basic operational modes of MRF: flow mode (i.e. valve mode), shear mode, squeeze mode [16-18]. These three modes normally comprise of pairs of parallel plates to form channels to accommodate MRF. The difference between them is the movement of plates: in flow mode, which is the most widely used, MRF flows between two stationary parallel plates under pressure drop when the magnetic fluxes pass perpendicular to the flow direction [19]. To increase the force output, a long flow channel is normally designed, which alleviates the viscous damping force hence compromised the MR effect. In shear mode, one plate moves relatively to another and deforms the MRFs [17]. Both flow and shear mode are frequently used because of simple design and easy manufacture [20]. MR devices with flow mode or shear mode are relative large in size to produce large force output and it is challenging to achieve miniaturization design [21]. In squeeze mode, one plate moves towards or opposites to the other to produce the flow and compressive deformation of MRF. Among the three operation modes, squeeze mode usually produces highest force and is particularly effective for applications with small-amplitude movement [17]. In addition, a high requirement of sealing technique is required due to large damping force generated MR devices base on squeeze mode.

Table 1. List of MRF mount designs in open literatures.

Max Force	Force increase	Mode	Max. magnetic flux density B	Power (current)	Reference
25.27 kN	233.31%	flow	radial:0.24~0.26T annular:1.6T	125W (2A)	[22]

25 kN	<100%	flow	radial:0.32~0.38T annular:0.86~0.94T	12.78W (1.4A)	[13]
24.55 kN	221.17%	flow& shear	radial:0.47T	(3A)	[23]
2.8 kN	185%	flow& shear	radial: ≈0.25T annular: ≈0.25T	(0.5A)	[24]
<0.02 kN	<400%	shear	-	(1A)	[25]
0.6 kN	<500%	squeeze	around 1.2T	(2A)	[26]

The combination of operating modes can combine the advantages of different modes. Mixed flow channel with both annular and radial channels is adopted by all above designs based on flow mode [13, 22-24, 27] to obtain high MR effect by maxmising the length of flow channel. To obtain high level of force output, the squeeze mode is the one to adopt in the design of heavy-duty MRF mount with mixed mode if the stroke of the device is not a concern. Another important factor is to design efficient magnetic flux path to generate high magnetic field in MR fluid to activate MR effect. As seen in Table 1, larger magnetic flux density B can effectively improve the adaptive range of force output. To achieve this, design of coil with sufficient provision of magnetic field should be considered including the selection of coil location and optimization of coil configuration. Among the above designs in Table 1, coil is put outside of the MR valve in [13, 25, 26], which could maximum the use of magnetic flux. Phu et al. [23] adopt multi-coils to generate large damping force, which increase the difficulty of design and manufacture.

In this paper, a MRF mount design with combined flow and squeeze mode is proposed to produce large force, high adaptive range and low power consumption. Finite element analysis, theoretical modelling and experimental testing were conducted to validate the design. The detailed structures are as follows: section 2 describes the

configuration and working principle of the proposed MRF mount; in section 3, the ANSYS Electronics Desktop is used to obtain magnetic field distribution in the valve. A mathematical model based on the Bingham model is constructed to predict the damping force of the proposed MRF mount; in section 4, static and dynamic tests of MRF mount under different conditions (frequency, amplitude, current) are conducted. Experimental results including effective stiffness and equivalent damping are analyzed, and the hysteretic behaviour in the experimental results is explained. Conclusive remarks are presented at the end of the paper.

2. The design of proposed MRF mount

2.1 Configuration of the MRF mount

The schematic of the proposed MRF mount is presented in **Error! Reference source not found.**(a), which consists of three main parts: rubber part, support part and MR valve. To provide enough stiffness under static loads, the rubber part is made of nitrile butadiene rubber (NBR) in cone shape. The support part is positioned above the rubber part to expand the contact area with loads of upper loads and to ensure that rod and rubber part can move synchronously. Figure 1(b) presents the schematic of the MR valve which is comprised of piston, rod (upper and lower parts), coil, separated ring, upper and base plates. The upper and base plates, made of AISI 1020 steel, constitute the housing together, allowing the piston to have a limited movement. Inside the housing, 2166 turns of Φ 0.75 mm copper wire is winded on the aluminum bobbin, and aluminum separated ring is set to ensure the piston movement smooth and straight.

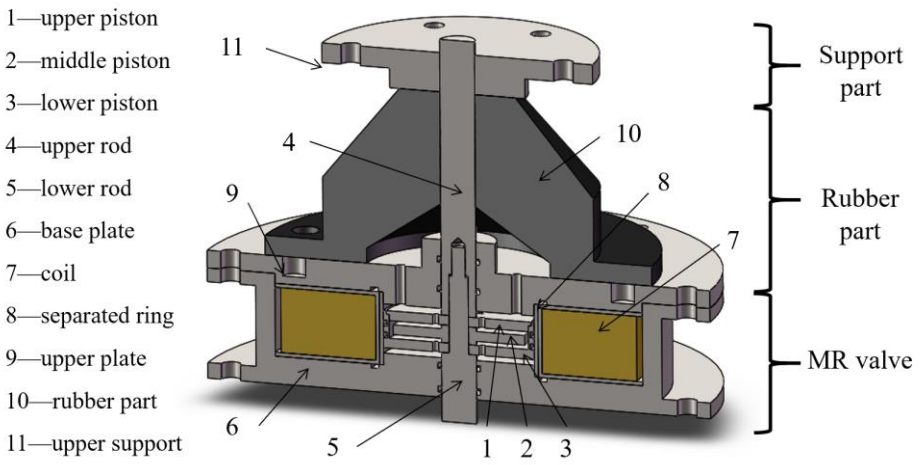

(a)

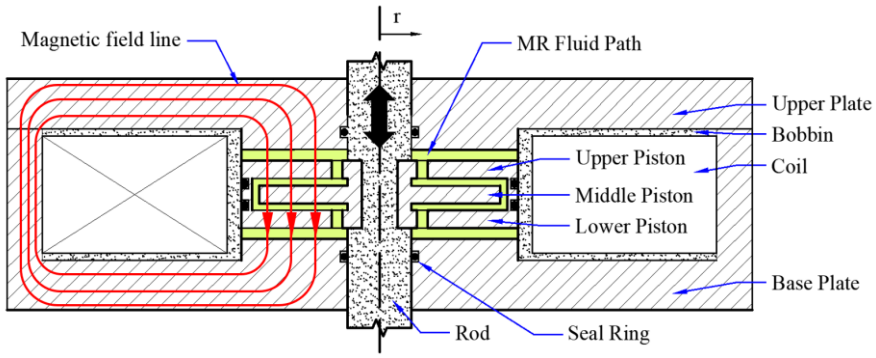

(b)

Figure 1. The schematic diagram of the proposed (a) MRF mount and (b) MR valve.

Traditional squeeze structure only uses one piston part, the magnetic circuit merely passes through the two squeeze regions on both sides, which does not fully utilise the magnetic flux. In the proposed MRF mount, the MR valve employs a new type of squeeze-flow-valve to form two symmetric radial flow channel to increase the use of magnetic flux. The piston consists three parts, which form a flow path with both annular and radial paths to increase the length of flow channel. Six orifices are arranged in the upper and lower parts to allow MRF flowing in the gaps. The upper and lower parts of rod, made of 304 stainless steel, could clamp these three parts of piston tightly. Moreover, to prevent the leakage of MR fluid, six NBR O-rings are used between the piston and separated ring, plates and rods. Table 2 summarized the materials of all

componentsTable 2.

Table 2. Summary of the component material.

Component	Material
Coil	Copper (Φ 0.75 mm)
Rod	304 stainless steel
Seal Ring	NBR
Bobbin	Aluminum
Middle Piston	AISI 1020
Down Piston	AISI 1020
Upper Piston	AISI 1020
Upper Plate	AISI 1020
Down Plate	AISI 1020
Separated ring	AISI 1020

The 50% iron particle weight fraction MRF (Shaanxi Xulihengxin Materials Co., Ltd, China) is used. The B-H hysteresis curve of MRF is presented in Figure 3(a). The MRF can produce up to 48 kPa yield stress under a magnetic field of 1.0 T. For a magnetic flux intensity of 0.7T, the yield stress is around 44 kPa. The relationship between yield stress (τ_y) and magnetic flux intensity (B) is described in equation(1) by using 4th order polynomial curve fitting method with the data obtained from manufacturers. The calculated relationship between τ_y and flux density (B) is shown in Figure 2.

$$\tau_y = 22.847 \times B^4 - 38.195 \times B^3 - 38.665 \times B^2 + 102.08 \times B + 0.0258(\text{kPa}) \quad (1)$$

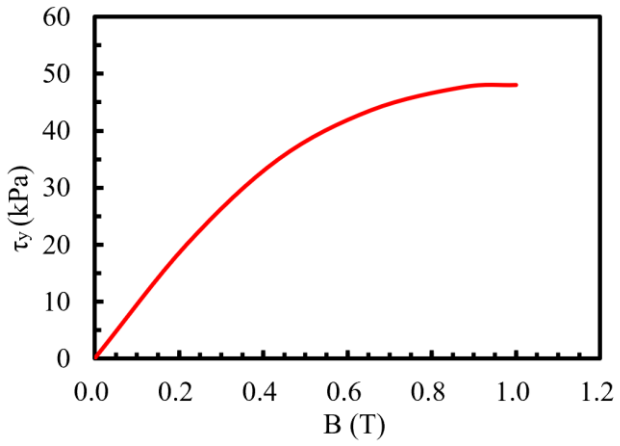

Figure 2. Yield stress versus the magnetic flux density of MRF

2.2 Principle of the MRF mount

The MRF mount is to isolate the vertical vibration by intelligently adapting the force output according to external excitation. When the vertical loading is applied to the mount, the rod and piston will move together to push MR fluid flowing through the channels. When the coil is energised, the generated magnetic field changes the yield stress of MRF and hence the damping force output of the MRF mount. The damping force includes contribution from by four parts: elastic force of rubber, friction, viscosity, and MR effect.

The flow channel is illustrated in Figure 5, consisting of two types of regions: squeeze region and flow region. Region 1 and region 4 are the squeeze regions, and the flow region is divided into radial path and annular path, which are region 2 and region 3, respectively. The annular and radial paths are parallel and perpendicular to the inlet and outlet of the valve, respectively [17].

Magnetic flux density in MRF path is affected by the size of effective path gap. In other word, a wider gap of MRF path leads to lower magnetic field intensity, and then decreases yield stress of MRF and controllable damping force. Hence, the gap in squeezed region h_0 and h_1 are chosen as 3mm initially. However, in fixed valve structure, small damping gap (less than 1.5mm) would cause a “block up” phenomenon, which could compromise the performance of MRF devices [20]. Therefore, the gap d_2 of flow path in piston adopts 2mm to prevent this phenomenon. The out diameter of MR valve

is 200mm, and the height of it is only 53mm, which is a relatively compact structure. Table 3 summarizes the specific dimensions and parameters of proposed MRF mount.

Table 3. Specification of the parameter of proposed MR valve.

Parameter	Symbol	Value	Unit
Thickness of upper plate	L_1	14	mm
Thickness of big piston	L_2	19	mm
Thickness of down plate	L_3	14	mm
Radius of rod	R_0	9	mm
Inner diameter of the hole	R_1	10.5	mm
Outer diameter of the hole	R_2	13.5	mm
Outer radius of middle piston	R_3	34	mm
Outer radius of big piston	R_4	39	mm
Upper initial gap	h_0	3	mm
Lower initial gap	h_1	3	mm
Diameter of outside annular path	d_0	3	mm
Thickness of upper piston	d_1	5	mm
Diameter of radial path	d_2	2	mm
Diameter of inside annular path	d_3	2	mm
Viscosity of MRF	η	0.112	Pa·s
Density of MRF	ρ	3.05	g/cm^3

3. Magnetic analysis and predictive modeling

3.1 Finite element analysis

Estimating the magnetic field distribution in the MR device is the fundamental step towards predicting the strength of the MR effect that can be produced by the MR materials[28]. ANSYS Electronics Desktop is used to construct the 2D symmetric finite element model and compute the magnetic field distribution in the proposed MR valve. The materials and dimensions of the valve components for the finite element model are summarized in Table 2 **Table 2**and Table 3, respectively. The B-H curves of MRF and AISI 1020 steel are presented in Figure 3(a) and (b). The relative permeabilities are set as 1 for copper and aluminum components, respectively.

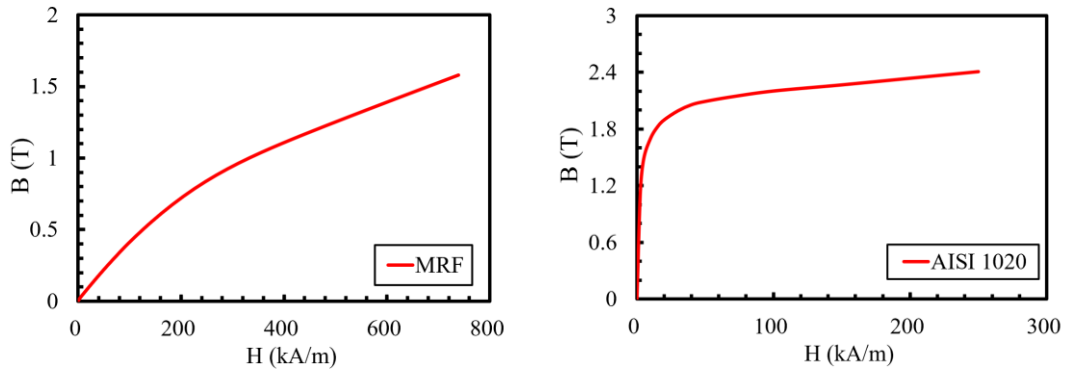

(a) (b)

Figure 3. B-H curve of (a) MR fluid and (b) AISI 1020.

The results of finite element analysis are shown in Figure 4. Here, the maximum amplitude is 2mm, it is necessary to verify the difference of magnetic flux density when the piston moves in different positions. Two different gap distances of squeeze region, i.e., 1mm and 3mm, are selected and presented as solid-line and dashed-line respectively in Figure 4(c-e). The simulation results of these two scenarios under 1A current applied are shown in Figure 4(a) and (b), respectively. Their detail distributions on line 1-3 are shown in Figure 4(c-e). Six lines are chosen to verify the distribution of magnetic flux density. Line 1 and line 4 are the magnetic flux density distributions in the middle of cross section of squeeze region. Line 2 and line 5 are that in the middle of cross section of radial flow region. Line 3 and line 6 are that of longitudinal section of entire liquid chamber.

In Figure 4(c) and (d), it can be seen that the magnetic flux densities of cross section in squeeze region and radial flow region are all uniformly distributed. In Figure 4(e), the magnetic flux density of line 3 and line 6 that passes through the liquid channel vertically are evenly distributed, indicating that a vertical chain structure can be formed under the action of magnetic field. It proves that the flux density in both squeeze and

flow region are rather uniform.

Compared with two different gap distances, the maximum values of magnetic flux density on line 1and line 4 are 0.742T and 0.775T, respectively. Similarly, in the flow region, the maximum B values are 0.7T and 0.705T on line 2 and line 4, respectively. It can be found that, under two different gap distances, the value of magnetic flux density has minimal variation in squeeze region, while that are almost unchanged in radial flow region. It can be concluded that the influence between different gap distance can be neglected.

It is worth noting that, the simulation results only provide a reference. Yazid et al[10, 29] propose that, in real test, clumping effect could appear in the squeeze regions, which means that magnetic particles may accumulate in squeeze region while carrier fluid with fewer iron particles flows during flow region[30]. Therefore, the clumping effect may affect the accuracy when comparing with experimental results.

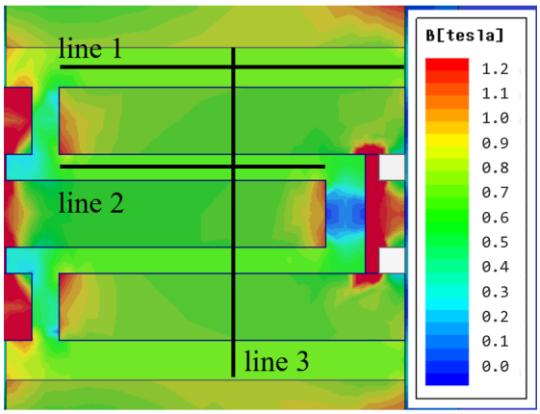

(a)

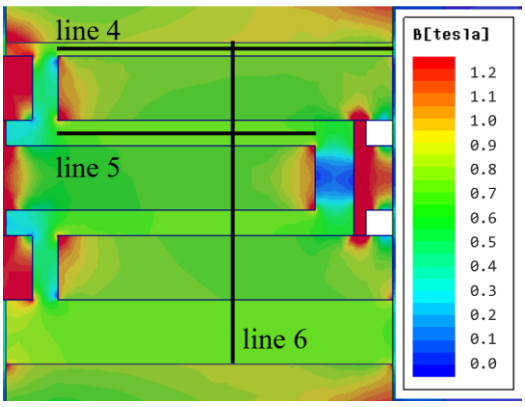

(b)

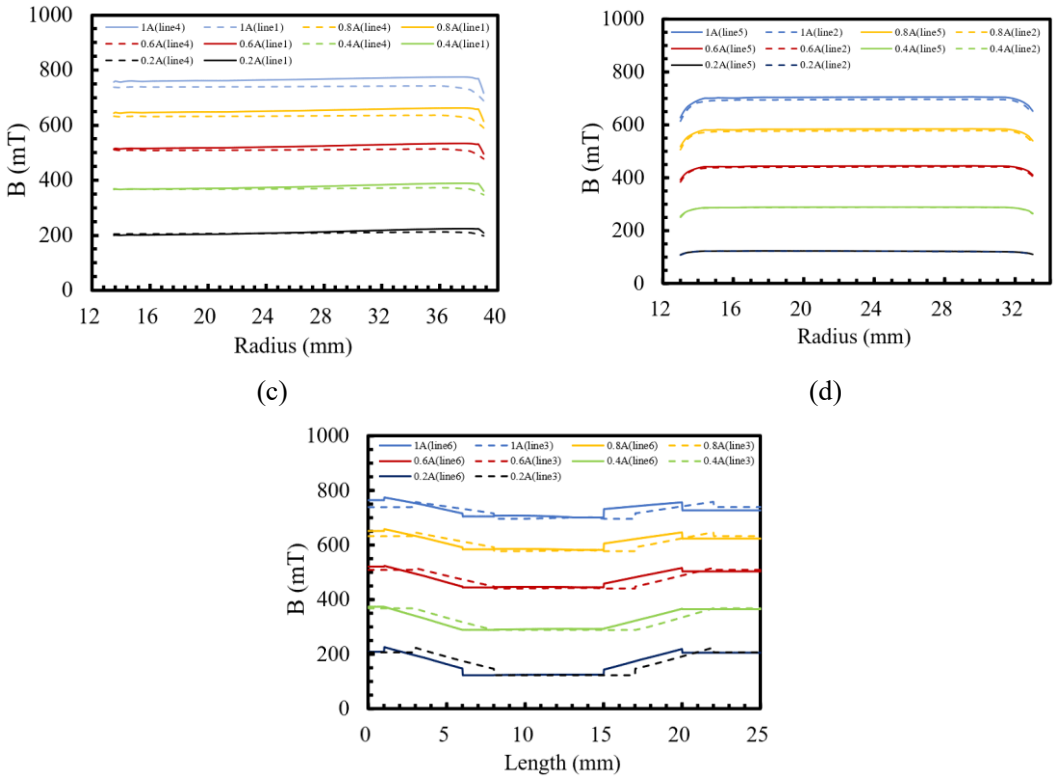

Figure 4. Magnetic field distribution of (a)3mm; and (b)1mm gaps under 1A; Magnetic flux strength under different current in (c)squeezed region(line1and line4); (d) flow region(line2 and line4); and (e)longitudinal profile(line3 and ling6).

3.2 Predictive modeling

In order to evaluate the performance of the structure before the test, this paper proposed a mathematical model to predict maximum damping force generated by MRF mount under different excitations.

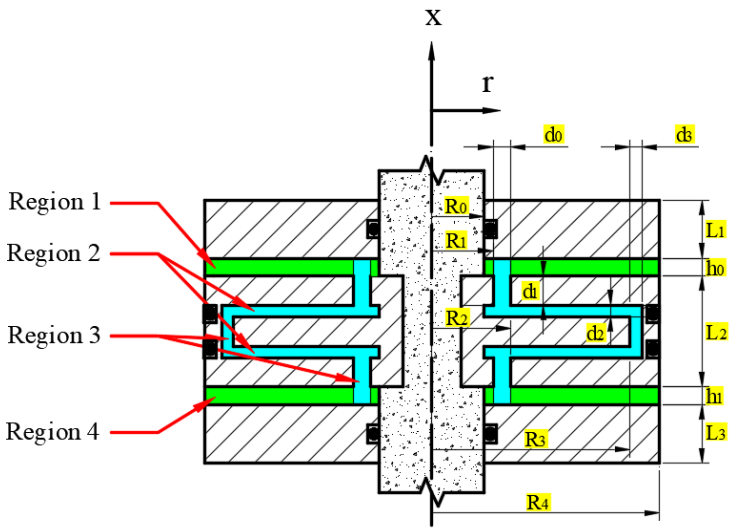

Figure 5. The parameterized model of the MR valve.

Here, before the model is built, assumptions and simplifications are made: (i) the entire channel is assumed to be filled with incompressible MR fluids, and only laminar flow occurs because of low Reynolds number [31]; (ii) the force due to the inertia of the MRF is neglected in this study because of small amount of MRF (about 46ml) and low frequency excitation (4Hz); (iii) the vertical pressure difference in the both paths is neglected; (iv) In squeeze region, the squeeze effect of inside area near the rod is neglected because the area is too small. Then, the total force transmitted by proposed MRF mount can be expressed by

$$F_{\text{total}} = F_{\eta} + F_{\text{mr}} + F_{r} + F_{f} \tag{2}$$

where F_{total} is the total damping force; F_{η} and F_{mr} represent the forces due to viscosity of the MRF and MR effect respectively; F_{r} represents the force produced by rubber part; and F_{f} represents friction in motion, mainly caused by the deformation of rubber sealing ring. These will be described in following sections.

3.3 Viscous force

The viscous force is determined by the properties of the MR fluid itself, regardless of the presence of a magnetic field. When the device moves smoothly, pressure difference will appear between the region 1 and region 4 as shown in Figure 5. In order to simulate viscous effect, the squeeze flow of MR fluids in region 1 and region 4 can be seem as no-slip pseudo-steady state due to low Reynolds number[26]. The viscous effects of the fluid in region 1 after simplified can be approximated by

$$P_{\eta 1}(r) = \frac{6\eta\dot{x}}{(h_0 - x)^3}\left(\frac{1}{2}\left(r^2 - {R_2}^2\right) - R_2^2(ln\, r - ln\, R_2)\right) \tag{3}$$

where $P_{\eta 1}$ is the pressure of viscous effect in region 1; η is the viscosity of MR fluids; $\dot{x}$ presents velocity of piston; h_0 and h_1 present the upper and lower initial gaps of squeeze regions. Similarly, the pressure distribution in region 4 can be derived as follows:

$$P_{\eta 4}(r) = \frac{6\eta\dot{x}}{(h_1 + x)^3}\left(-\frac{1}{2}\left(r^2 - {R_2}^2\right) + R_2^2(ln\, r - ln\, R_2)\right) \tag{4}$$

Due to the structure inside the piston is symmetrical, according to [18] and [17], the viscous pressure drops of radial and annular ducts in MR valve can be obtained as follows respectively:

$$\Delta P_{\eta 2} = 2 \times \frac{6\eta Q}{\pi d_2^3} \cdot ln\frac{R_3}{R_2} \tag{5}$$

$$\Delta P_{\eta 3} = 2 \times \frac{6\eta Q \cdot (d_1 + d_2)}{\pi d_0^3 (R_1 + d_0/2)} + \frac{6\eta Q \cdot (L_2 - 2d_1 - 2d_2)}{\pi {d_3}^3 (R_3 + d_3/2)} \tag{6}$$

$$Q = \dot{x} A_p \tag{7}$$

$$A_p = \pi(R_4^2 - R_0^2) \tag{8}$$

where d_2 is the thickness of radial duct; d_1 is the thickness of upper piston also the

length of outside annular path; Q is the flow rate which can be presented by the piston velocity $\dot{x}$ and piston area A_p in equation (7) and (8). d_0 and d_3 are inside and outside diameter of annular paths, respectively. Therefore, the total viscous force can be calculated as:

$$\begin{aligned} F_\eta(x,\dot{x}) &= \int_{R_2}^{R_4} 2\pi r \cdot \left[P_{\eta 1}(r) - P_{\eta 4}(r)\right]dr + A_p \times \left(\Delta P_{\eta 2}(r) + \Delta P_{\eta 3}(r)\right) \\ &= \left[\frac{12\pi\eta\dot{x}}{(h_0 - x)^3} + \frac{12\pi\eta\dot{x}}{(h_1 + x)^3}\right] \cdot \left[\frac{1}{8}\left({R_4}^4 - {R_2}^4\right) - \frac{1}{2}{R_2}^2{R_4}^2(ln\, R_4 - ln\, R_2)\right] \\ &+ 6\eta Q\left[2 \times \frac{1}{\pi d_2^3} ln\frac{R_3}{R_2} + 2 \times \frac{(d_1 + d_2)}{\pi d_0^3\left(R_1 + \frac{d_0}{2}\right)} + \frac{(L_2 - 2d_1 - 2d_2)}{\pi {d_3}^3\left(R_3 + \frac{d_3}{2}\right)}\right] \times A_p \end{aligned} \quad (9)$$

3.4 Force due to MR effect

The force F_{mr} only occurs when the magnetic field is applied, which depends on the MR effect. When the coil is activated, region 1 and region 4 will generate squeeze effect, and the flow effect is generated on the region 2. It can be seen in Figure 1(b) that the magnetic field flux lines pass parallelly to the both outer and inner annular regions, hence the MR effect would not appear there. Therefore, this section is divided into two parts of squeeze and flow to describe respectively.

In finite element analysis, it can be found that the flux density in both squeeze and flow region are rather uniform, hence the uniformed magnetic flux intensity can represent the entire squeezed region. Same principle applies to flow region. Here, the values $\tau_1(B)$ and $\tau_2(B)$ represent the flux density in squeeze and flow region respectively. Considering that MR fluids are typical Bingham fluids, and assuming that the flow occurs near the outside annular ducts, the pressure gradient $\frac{\partial P_{\text{mr}}}{\partial r}$ in region 1 can be expressed as [19, 31, 32]:

$$\frac{\partial P_{\text{mr}}}{\partial r} = -\frac{2\tau_{y1}}{h_0 - x} sign(\dot{x}) \tag{10}$$

where τ_y is the yield stress of MRF; $\dot{x} > 0$ stands for the upwards movement of the piston. When the MR fluid is squeezed, the yield stress of the MR fluid will increase because the curved chain structure forms a stronger chain, which is more difficult to break [19]. So Tao et al. [33] proposed an empirical expression that related the shear yield stress τ_y to the normal stress P_{MR}:

$$\tau_{\text{y1}} = \tau_1(B) + K_H P_{\text{MR}} \tag{11}$$

where K_H is a multiplication factor increasing with the magnetic field. Substituting Equation (11) into Equation (10), then integrating with respect to radius *r*, with assumption that the free boundary ($P_{\text{MR}}(R_2) = 0$), the pressure due to the squeezed MR effect can be described by

$$P_{mr} = \frac{\tau_1(B)}{K_H}\left[e^{\left(\frac{2K_H(R_4 - r)}{h_0 - x}\right)} - 1\right] \tag{12}$$

The pressure drop of the radial flow path due to MR effect can be described as [17, 18, 23, 27]

$$\Delta p_{\text{mr}} = \frac{c_1 \tau_2(B)}{d_2} \cdot (R_3 - R_2) \tag{13}$$

where c_1 is a coefficient function determined by yield stress, and can be approximated as follows:

$$c_1 = 2.07 + \frac{12Q\eta}{12Q\eta + 0.8\pi\left(\frac{R_2 + R_3}{2}\right){d_2}^2 \tau_2(B)} \tag{14}$$

The total force due to MR effect is expressed as follow:

$$F_{mr} = \& \int_{R_2}^{R_4} 2\pi r \cdot P_{mr} dr + \Delta p_{\mathrm{mr}} A_{up}\, sgn(v)$$

$$= \pi\tau_1(B)\left[\frac{{R_4}^2 - {R_2}^2}{K_H} - \frac{R_4(h_0 - x)}{{K_H}^2} + \frac{R_2(h_0 - x)}{{K_H}^2} e^{\left(\frac{2K_H(R_4 - R_2)}{h_0 - x}\right)} - \frac{(h_0 - x)^2}{2{K_H}^3} + \frac{(h_0 - x)^2}{2{K_H}^3} e^{\left(\frac{2K_H(R_4 - R_2)}{h_0 - x}\right)}\right] \quad (15)$$

$$+2 \times \frac{c_1\tau_2(B)}{d_2} \times (R_3 - R_2) \cdot A_{up}\, sgn(v)$$

3.4 Rubber part and friction

The proposed MRF mount has an initial stiffness under static load, mainly due to the rubber part. Under static and low frequency loads, rubber is recognized as elastic element, expressed as.

$$F_r = k_r x \quad (16)$$

where k_r and x presents equivalent stiffness of rubber part and displacement of piston rod respectively.

Due to the use of O-rings made of NBR, friction is within the total damping force in the test. The friction is presented as a constant value *f* independent of displacement [42].

$$F_f = f \times sign(\dot{x}) \quad (17)$$

However, the constant value *f* is difficult to be estimated theoretically. In addition, in order to get the accurate performance of the MRF mount, the stiffness of rubber part k_r also has to be measured during experiment in section 4, though it has a designed stiffness of about 0.5kN/mm during the fabrication.

3.5 Prediction of the output force

In order to predict the performance of proposed effective structure, an approximate value of maximum damping force should be calculated using the equation (2) of the

established mathematic model with all parameters list in Table 2 and Table 3. Here, $\tau_1(B)$ and $\tau_2(B)$ is calculated by equation(1) with the magnetic flux density B from FEMM simulation results. The stiffness of rubber part k_r and friction constant f are 0.57kN/mm and 1kN respectively, based on experimental measurements of a fabricated prototype referring to section 4.1.

Figure 6 shows the results of predicted damping force under 1Hz frequency with different amplitudes (1, 1.5 and 2 mm) when 1A current is applied. The damping force has a large growth with increasing current. The maximum damping forces are 14kN, 15.1kN and 17.42kN, respectively. Compared with the case without current applied, the calculated force increases are 685%, 687% and 767%, respectively, which states that the proposed MRF mount could generate high damping force with large adjustable range thus would be an ideal candidate for vibration reduction of heavy-duty applications.

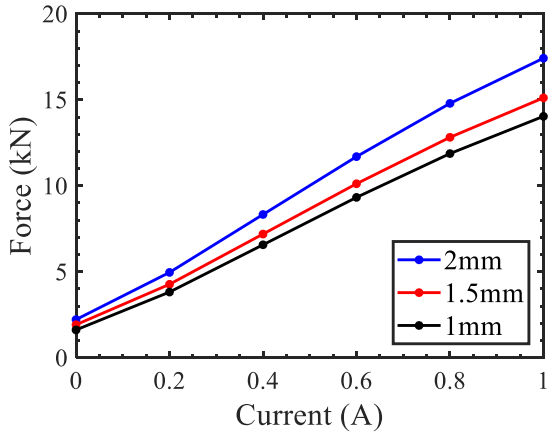

Figure 6. Predicted maximum force at 1Hz under different amplitudes.

4. Experimental testing

4.1 Experimental setup

To evaluate the performance of proposed MRF mount, a prototype was designed and manufactured. The components and assembly of the prototype is manufactured as shown in Figure 7(a) and (b).

The experimental apparatus and setup to test the performance of the MRF mount are presented in Figure 7(c), including one DC power supply (IT6830A, Itech Electronic, Co., Ltd., USA), a data acquisition system and a servo hydraulic fatigue stretcher (Instron-8802, Instron, Co., Ltd., USA). As shown in the Figure 7(c), displacement was controlled by the system using computer, and the damping force of the MRF mount is measured by a load cell built in Instron tester. The load cell measures the damping force outputs at the sampling rate of 512 Hz.

The MRF is injected into the prototype using a pump. During injection, the piston is moved back and forth to eliminate air in the channels. Then the bottom and top of the MRF mount are connected with the test equipment. The MRF mount was trialed for 5 minutes to ensure good dispersion of the magnetic particles inside the MRF.

Then in the dynamic experiment, MRF mount is excited with the frequency of 0.1Hz, 1.0 Hz, 2.0 Hz, and 4.0 Hz sine waves, the excitation amplitudes are chosen as 1.0 mm, 1.5mm and 2.0 mm, and the range of applied current is from 0 to 1A with a step of 0.2A. To guarantee the reproducibility of the experiments, each test was repeated for 20 cycles.

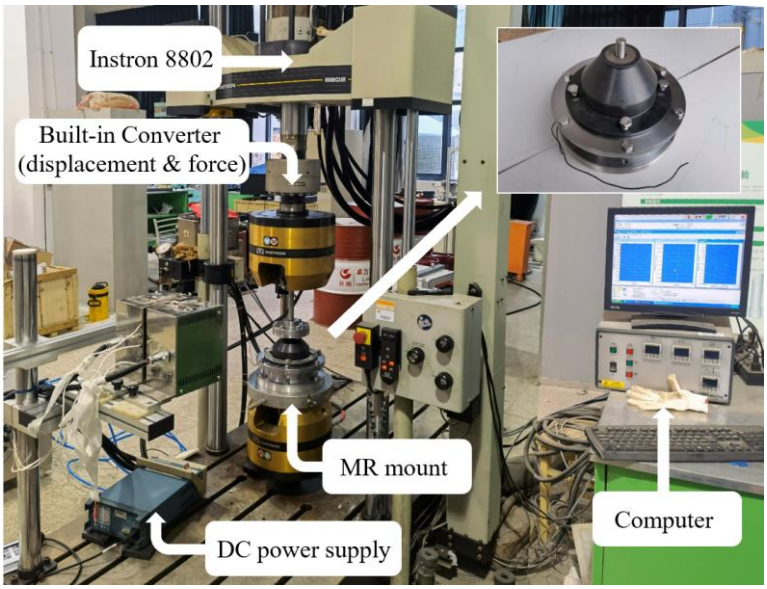

Figure 7. Photograph of experimental setup for the proposed MRF mount.

4.2 Static test result of Rubber part

The proposed MRF mount works under static load carried by the rubber part. Therefore, before the dynamic test, a static test was set up to obtain the stiffness of rubber part. The load is input by computer to reach the target value at the rate of 0.025 mm/s. The deformation was obtained after 40 s when each load has applied. Figure 8 shows the test results of rubber part, in which force–displacement loop shows a linear relationship. The equivalent stiffness can be obtained as about 0.57 kN/mm in Figure 8. This value provides guidance for the theoretical model.

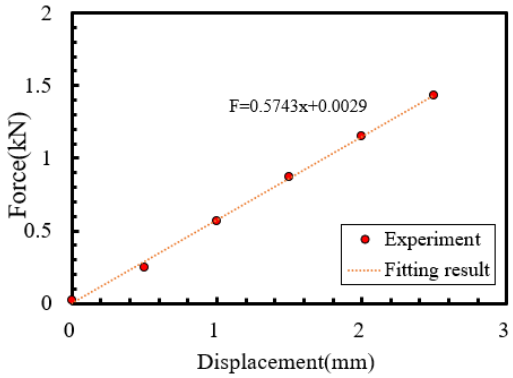

Figure 8. Static experimental and fitting results of rubber part

4.3 Dynamic test results

4.3.1 hysteresis characteristics

Before the dynamic test, a 1.8kN load is applied to keep the piston in the central position with upper and lower initial gaps of about 3mm due to static deformation of rubber part. It is worth noting that, to describe the performance of MRF mount more accurately, the static force generated by the rubber part has been removed in the following figures.

The off-state damping force is tested to identify the zero-field damping force characteristics. **Error! Reference source not found.** shows the diagram with different amplitudes under quasi-static condition (0.1Hz). It is worth noting that, because viscous force is linearly proportional to the piston velocity, demonstrating typical viscous behaviour, and friction is described as a constant f in equation (17), the quasi-static test could obtain the friction f by subtracting force rubber part produced from the results. The maximum force under 1.0 mm, 1.5mm, 2.0 mm are 1.59kN, 1.97kN and 2.3kN, respectively. It can be found that the Y-intercepts of the curves in **Error! Reference source not found.** are almost unchanged, hence the friction can be estimated as 1kN to guide the theoretical model.

Error! Reference source not found. presents the results without current applied under 2.0 mm amplitude and different frequencies (0.1Hz, 1.0 Hz, 2.0 Hz and 4.0 Hz). Comparing four force-displacement loops, it can be found that with increasing frequency, the slopes of the hysteresis loops remain almost unchanged. The maximum damping force are 2.30 kN, 2.53kN, 2.56kN and 2.63kN, respectively. Though viscous

force is positively correlated to the velocity, this phenomenon indicates that the off-state damping force is insensitive to the frequency change.

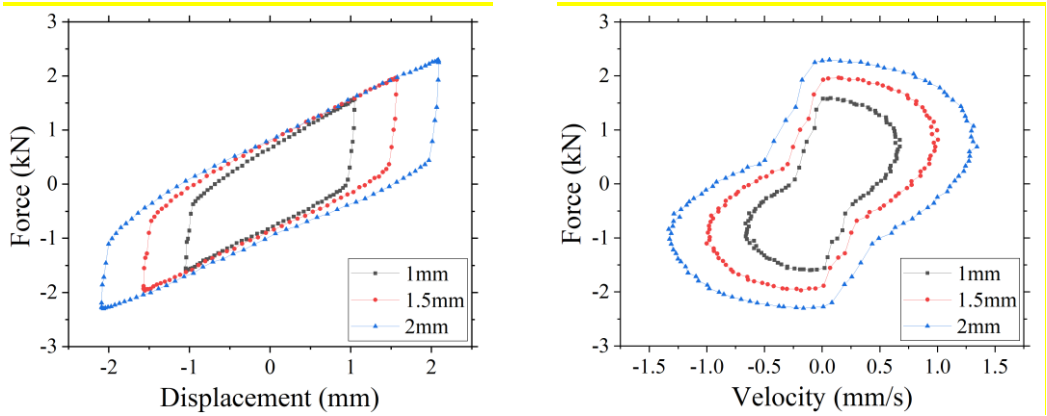

Figure 9. Zero-field force–displacement and force–velocity loops under different amplitudes at quasi-static frequency (0.1Hz).

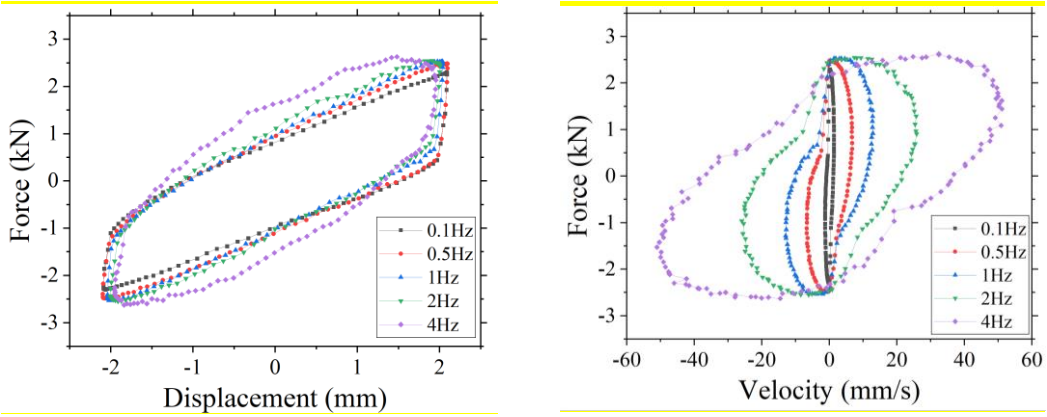

Figure 10. Zero-field force–displacement and force–velocity loops under different frequencies at 2.0 mm amplitude.

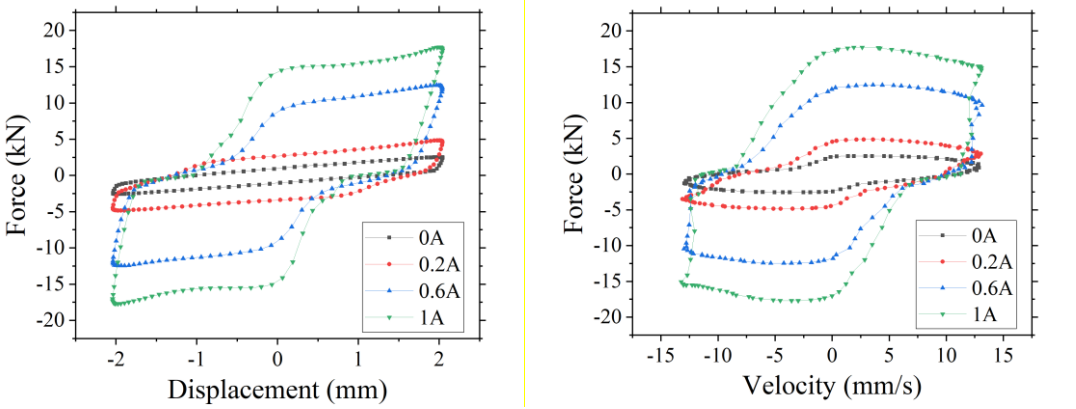

Figure 11. Force–displacement and force–velocity loops under different current applied at an amplitude of 2.0 mm and a frequency of 1.0 Hz.

As shown in Figure 11, the damping force grows acutely with the increase of applied current. A clear MR effect is observed hence large adaptive range is achieved.

For example, when 1.0 A current is applied, the damping force is approximate 7 times higher than that without current applied, under 2.0 mm amplitude and 1.0 Hz frequency. Compared to the viscous effect, the MR effect plays a major role in the damping force. The adjustability of damping force output under different conditions are list in Table 4.

$$Force\ \ increase(\%) = \frac{F_{\max} - F_{\text{off-state}}}{F_{\text{off-state}}} \times 100\% \tag{18}$$

where force increase indicates the adjustable range defined by the damping force with 1A current applied and without current applied.

It can be concluded that the force increase value becomes smaller with increasing frequency and amplitude. This can be easily explained by equation(5)(2)(9), that the viscous force has grown with the increase of amplitude and frequency. Since the force due to MR effect is only dependent on the amplitude in equation(15), with the increase of the amplitude and frequency, the proportion of viscous force in total damping force is increasing, which leads to the reduction of adaptive range.

Table 4. Ratios of controllable performance of MRF mount in test range.

Amplitude(mm)	Frequency(Hz)	Force increase(%)
1.0	0.1	822.7
	1	714.4
	2	712.5
	4	687.2
1.5	0.1	757.9
	1	660.9
	2	666.8
	4	646.3
2.0	0.1	719.3
	1	600.4
	2	594.5
	4	575.7

Figure 12 compares the damping forces at the excitation frequencies from 0.1Hz

to 4.0 Hz under 1.0 mm and 2.0 mm amplitudes when the applied current is 1.0 A. The measured maximum damping forces under 1mm amplitude are 14.67kN, 13.36kN, 12.97kN and 14.84kN, respectively. Under 2mm amplitude, they are 18.84kN, 17.72kN, 17.71kN and 17.77kN, respectively, which indicates that frequency has minor effect on the maximum damping force. According to the equation (2), it can be found that the damping force is positively correlated to the frequency. The reason on a higher value in 0.1Hz is that rubber part has pronounced hysteresis and does not return all the absorbed compression energy on the rebound.

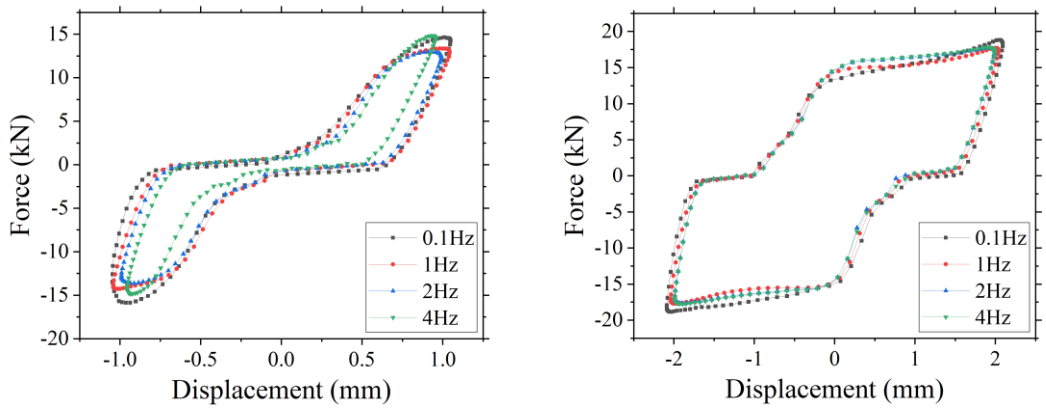

Figure 12. Experimental results with 1A current under (a) 1mm and (b)2mm amplitude.

Figure 13 shows the experimental results under 1.0 Hz sinusoidal inputs with different amplitudes (1.0 mm, 1.5 mm and 2.0 mm) when 1.0 A current applied. The maximum values of damping force are 13.36 kN, 15.56 kN and 17.72 kN, respectively. The damping force is more sensitive to amplitude than frequency. And it can be found that the experimental results could agree well with predicted results shown in Figure 6.

A noteworthy phenomenon is the pinching of the hysteretic curves among the experimental results shown in Figure 11-13. With the increase of displacement, force has a large growth after passing a certain displacement value and vice versa. It can be

deduced that the force due to flow is obviously small when displacement is under certain threshold, and MRF chains are not yield, which can neglect flow effect at this time. In addition, the damping force produced by squeeze effect is really small because of short squeeze distance. When the displacement increases gradually, with the squeezed distance increases, MRF begins to flow, and damping force significantly increases due to obvious squeeze and flow of MR effect.

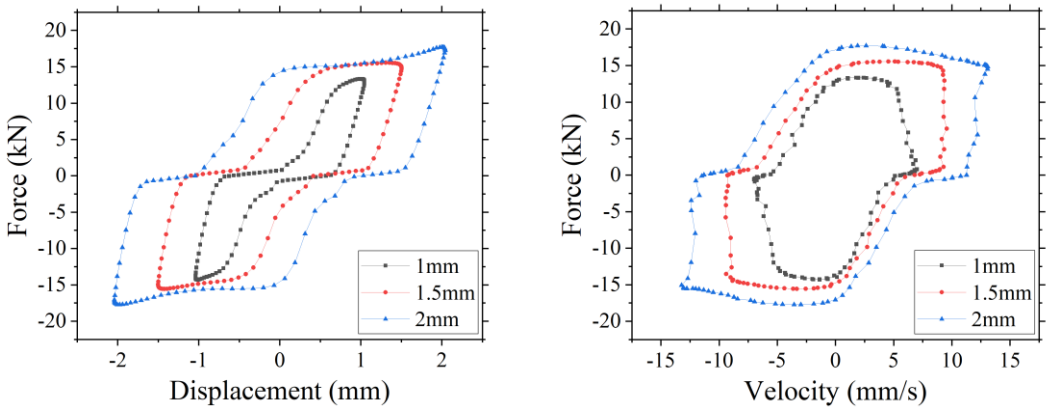

Figure 13. Experimental results under 1Hz with 1A applied current at a frequency of 1.0Hz

4.3.2 Effective stiffness

The effective stiffness is a parameter to evaluate the stiffness effect of MRF mount, which can be obtained from the force-displacement loops according to equation(19)[34].

$$K_{\text{eff}} = \frac{F_{\text{dmax}} - F_{\text{dmin}}}{\Delta_{max} - \Delta_{min}} \tag{19}$$

where F_{dmax} is the force at maximum displacement (Δ_{max}) based on hysteretic loops, and F_{dmin} is the force at minimum displacement (Δ_{min}) based on hysteretic loops.

Figure 14 shows the results of effective stiffness under different frequencies, while the amplitude are 1.0 mm, 1.5 mm and 2.0 mm, respectively. It can be found that, when the input current changes, the effective stiffness almost remains unchanged, which can be characterized by Figure 14(c) under the amplitude of 2.0 mm. The fluctuation of the

effective stiffness in the case of high current input at 1.0 mm and 1.5 mm may be due to the low control accuracy at low amplitude. This also confirms that the MRF mount proposed in this paper is insensitive to frequency changes.

Figure 15 shows the variation of effective stiffness versus the applied current, indicated that the effective stiffness almost remains linear relationship with the current. For a given applied frequency, the relative increase of the effective stiffness varies from 600% to 800%. The specific values of the effective stiffness in all test conditions are listed in Table 5. At an amplitude of 1.0 mm, for a given test frequency, the effective stiffness increases vary from over 730% to 805%. While at an amplitude of 1.5 mm, the effective stiffness increases vary from over 642% to 705%. While at an amplitude of 2.0 mm, the increase values vary from over 642% to 705%. It can be found that with the test amplitude increasing, the effective stiffness increment decreases.

Comparing the value of effective stiffness under different test amplitude at a given frequency and applied current in Table 5, it can be seen that the effective stiffness decreases with the increase of amplitude. This is mainly due to that rubber elastic force contributed a very largest portion of the stiffness without current applied. The stiffness provided by the rubber part does not change with the current. It can also be concluded that the increase level is sufficient to confirm the MRF mount proposed in this paper being used as a vibration isolator for heavy-duty applications.

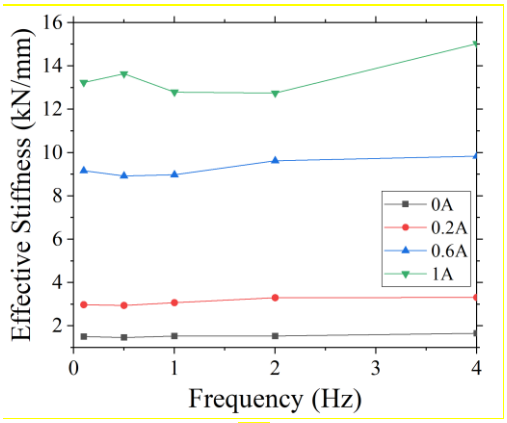

(a)

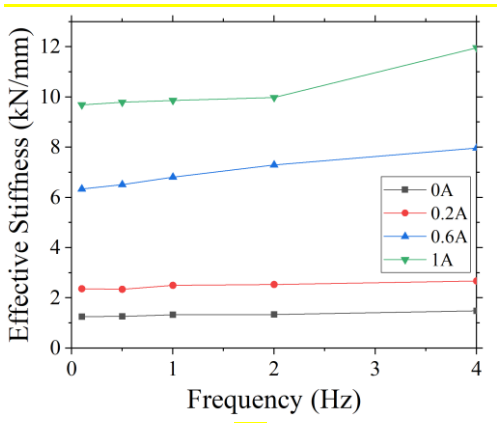

(b)

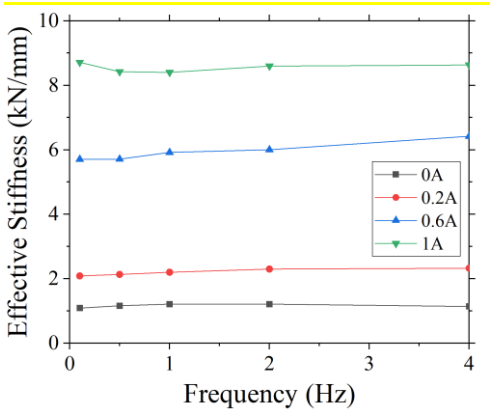

(c)

Figure 14. Effective stiffness for various frequencies with different amplitudes of (a) 1.0mm; (b) 1.5mm; (c) 2.0mm.

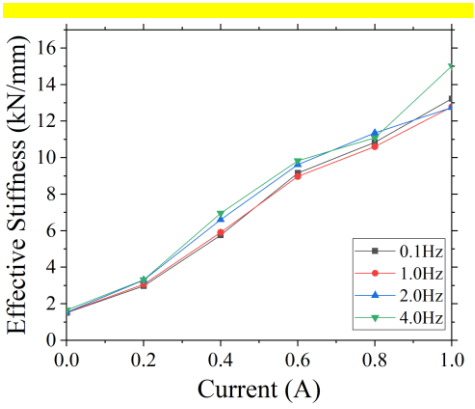

(a)

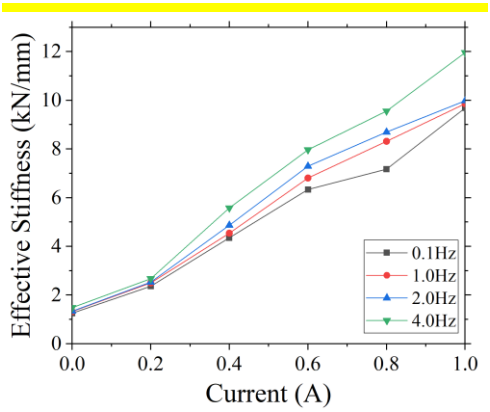

(b)

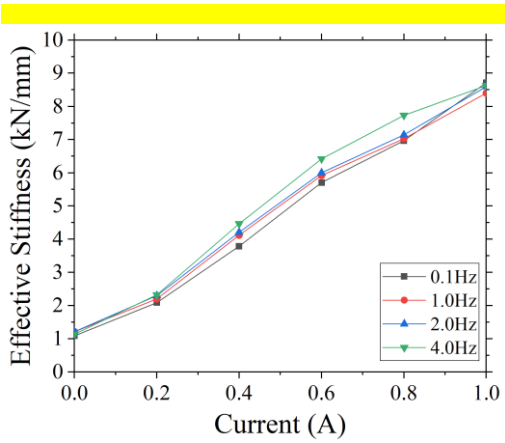

(c)

Figure 15. Effective stiffness for various applied currents with different amplitudes of (a) 1.0mm; (b) 1.5mm; (c) 2.0mm.

Table 5. Effective stiffness (kN mm^{-1}) of the MRF mount under different conditions.

Amplitude (mm)	Frequency (Hz)	Current (A)				Increase (%)
		0.0	0.2	0.6	1.0	
1.0	0.1	1.508252	2.979924	9.161405	13.23378	777.4246
	1	1.531956	3.069689	8.974604	12.78519	734.5662
	2	1.534388	3.300388	9.620824	12.74602	730.6909
	4	1.659657	3.313277	9.831813	15.02214	805.1352
1.5	0.1	1.257946	2.366338	6.338976	9.687042	670.0683
	1	1.32766	2.501143	6.807701	9.863328	642.9108
	2	1.340428	2.535649	7.292897	9.978382	644.4177
	4	1.48573	2.675024	7.966239	11.96038	705.0173
2.0	0.1	1.08969	2.088752	5.708492	8.713267	699.6094
	1	1.212969	2.202194	5.920291	8.401553	592.6438
	2	1.214128	2.300462	6.001681	8.595749	607.9773
	4	1.139287	2.325159	6.419672	8.629446	657.4426

4.3.2 Equivalent damping

To examine the performance of the MRF mount in energy dissipation, the equivalent damping is used in this section. The equivalent damping can be expressed as [34, 35]:

$$C_{eq} = \frac{EDC}{2\pi^2 f \Delta^2} \tag{20}$$

where EDC is the energy-dissipated, or the area of the hysteresis loop on every stable cycle in a given condition, f is the test frequency and Δ is the test amplitude.

Figure 16 and 17 show the equivalent damping subjected to different test frequencies and applied currents for amplitudes of 1.0 mm, 1.5 mm and 2.0 mm. It is obvious that the values of equivalent damping decreases exponentially with test frequency, but increases linearly with applied current. Table 6 lists the calculated value of the equivalent damping in all test conditions.

In general, for different amplitudes, the equivalent damping value decreases linearly with amplitude. The hysteresis loops between the equivalent damping and applied currents remains similar. For a given frequency at an amplitude of 1.0 mm, the relative increase of the equivalent damping is from about 296% to 567%. While for an amplitude of 1.5 mm, the relative increase varies from about 463% to 837%. While for an amplitude of 2.0 mm, the relative increase varies from about 610% to 920%. It can be found that the damping increment increases when the test amplitude increases, and it decreases with test frequency.

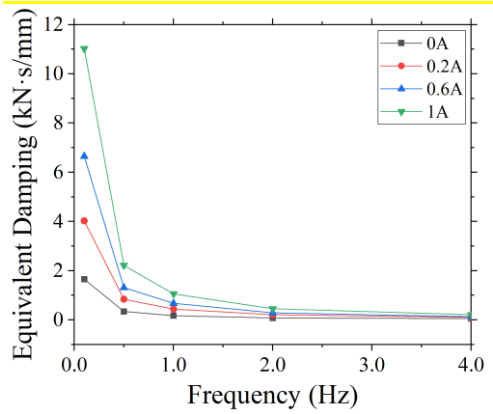

(a)

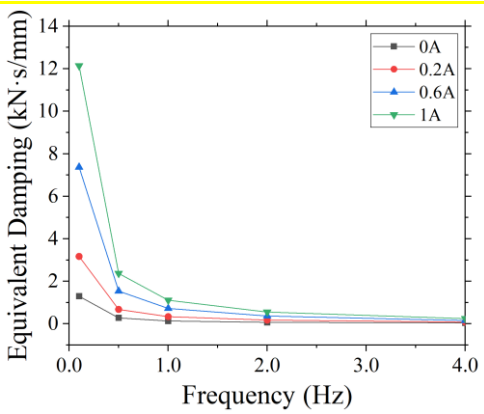

(b)

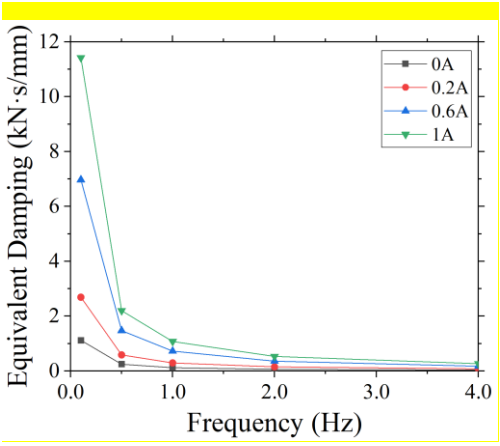

(c)

Figure 16. Equivalent damping for various frequencies with different amplitudes of (a) 1.0mm; (b) 1.5mm; (c) 2.0mm.

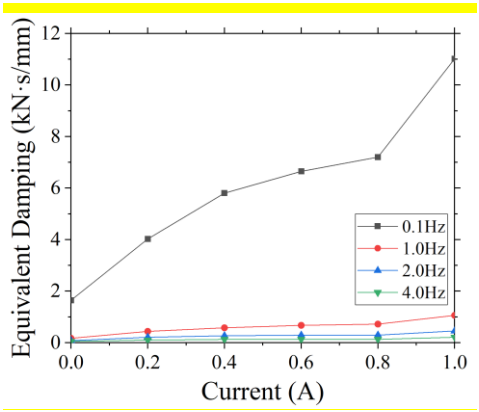

(a)

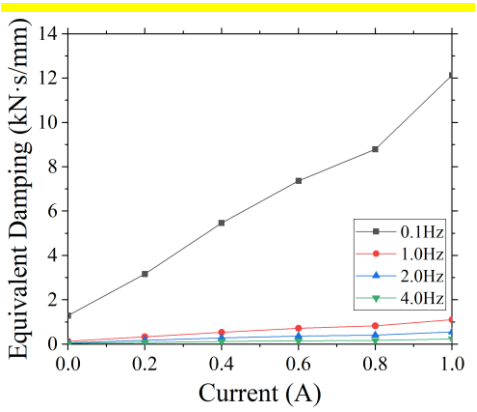

(b)

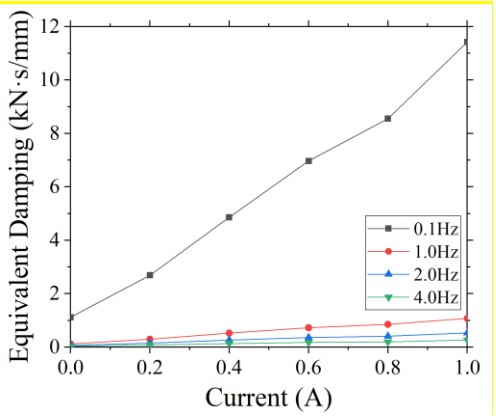

(c)

Figure 17. Equivalent damping for various applied currents with different amplitudes of (a) 1.0mm; (b) 1.5mm; (c) 2.0mm.

Table 6. Equivalent Damping (kN s mm^{-1}) of the MRF mount under different conditions.

Amplitude (mm)	Frequency (Hz)	Current (A)				Increase (%) (0-1A)
		0.0	0.2	0.6	1.0	
1.0	0.1	1.651181	4.028363	6.650226	11.01968	567.3816
	1	0.174223	0.441869	0.677193	1.06116	509.0802
	2	0.082542	0.215003	0.290351	0.457312	454.0387
	4	0.053983	0.106495	0.131248	0.213629	295.7352
1.5	0.1	1.295358	3.168881	7.370085	12.13538	836.8367
	1	0.132834	0.335524	0.722696	1.109932	735.576
	2	0.069182	0.176556	0.368499	0.553913	700.6553
	4	0.043068	0.083105	0.154425	0.242342	462.6974
2.0	0.1	1.119951	2.689145	6.971893	11.418	919.509
	1	0.122495	0.296252	0.726722	1.077172	779.3585
	2	0.064434	0.154153	0.358993	0.533829	728.4935
	4	0.037787	0.079945	0.177912	0.268258	609.9287

5. Conclusions

This study proposes a new MRF mount with large controllable range which can be an ideal candidate for vibration reduction of heavy-duty machines and infrastructures. The design of MRF mount with both annular and radial flows is based on two operating modes o: flow mode and squeeze mode. To maximize the magnetorheological effect of flow mode, flow channel consists of annular and radial paths. Finite element analysis is carried to provide strong and uniform magnetic field distribution in the valve. The squeeze and flow regions can obtain magnetic field intensities up to 0.742 T and 0.7 T under 1A current, respectively. A mathematic model is constructed to predict the maximum damping force output of the proposed device.

The experimental results show that the proposed MRF mount is sensitive to displacement than frequency. When no current applied, viscous force can be almost neglected, the off-state damping force is mainly comprised of elastic force by rubber

part and friction. When applied current, proposed MRF mount could generate high damping force with large adjustable range. The damping force at 1A can reach 18.843kN when the amplitude is 2mm and frequency is 0.1Hz, which has 719% increase of that without current applied. And under this condition, the effective stiffness increase and equivalent damping nearly up to 700% and 920%, respectively, which indicate that the proposed MRF mount is a variable stiffness and damping device with a large adjustable range. The test results have demonstrated the feasibility and potential of the proposed MRF mount for heavy-duty applications.

References

[1] Do Xuan Phu, Kruti Shah, Seung Bok Choi, Design of a new adaptive fuzzy controller and its implementation for the damping force control of a magnetorheological damper, Smart Materials and Structures 23(6) (2014).

[2] Huixing Wang, Tianxiao Chang, Yancheng Li, et al., Characterization of nonlinear viscoelasticity of magnetorheological grease under large oscillatory shear by using Fourier transform-Chebyshev analysis, Journal of Intelligent Material Systems and Structures (2020).

[3] Shaoqi Li, Tingting Tian, Huixing Wang, et al., Development of a four-parameter phenomenological model for the nonlinear viscoelastic behaviour of magnetorheological gels, Materials & Design 194 (2020).

[4] Quoc-Hung Nguyen, Seung-Bok Choi, Optimal design of a vehicle magnetorheological damper considering the damping force and dynamic range, Smart Materials and Structures 18(1) (2009).

[5] Şevki Çeşmeci, Tahsin Engin, Modeling and testing of a field-controllable magnetorheological fluid damper, International Journal of Mechanical Sciences 52(8) (2010) 1036-1046.

[6] B.F. Spencer Jr G. Yang, J.D. Carlson , M.K. Sain, Large-scale MR fluid dampers: modeling and dynamic performance consideration, Engineering Structures 24 (2002).

[7] Mauricio Zapateiro, Hamid Reza Karimi, Ningsu Luo, et al., Semiactive Backstepping Control for Vibration Reduction in a Structure with Magnetorheological Damper Subject to Seismic Motions, Journal of Intelligent Material Systems and Structures 20(17) (2009) 2037-2053.

[8] T Lee, K Kawashima, Semi-active control of seismicexcited nonlinear isolated bridges, Proc. 8th US National Conference on Earthquake Engineering, San Francisco, California, USA, 2006, pp. 421-429.

[9] Hyung-Jo Jung Kang-Min Choi , Sang-Won Cho , In-Won Lee, Application of Smart Passive Damping System Using MR Damper to Highway Bridge Structure, Journal ofMechanical Science and Technology 21(6) (2007) 870-874.

[10] Fitrian Imaduddin, Saiful Amri Mazlan, Hairi Zamzuri, et al., Design and performance analysis of a compact magnetorheological valve with multiple annular and radial gaps, Journal of Intelligent

Material Systems and Structures 26(9) (2015) 1038-1049.
[11] I. Saidi, E. F. Gad, J. L. Wilson, et al., Development of passive viscoelastic damper to attenuate excessive floor vibrations, Engineering Structures 33(12) (2011) 3317-3328.
[12] Iván M. Díaz, Paul Reynolds, On-off nonlinear active control of floor vibrations, Mechanical Systems and Signal Processing 24(6) (2010) 1711-1726.
[13] D. X. Phu, S. B. Choi, Y. S. Lee, et al., Design of a new engine mount for vertical and horizontal vibration control using magnetorheological fluid, Smart Materials and Structures 23(11) (2014).
[14] Nagi G Naganathan Yunhe Yu, Rao V Dukkipati, A literature review of automotive vehicle engine mounting systems, Mechanism and Machine Theory 36(1) (2001).
[15] Saravanan M. Peelamedu Yunhe Yu, Nagi G. Naganathan,Rao V. Dukkipati, Automotive Vehicle Engine Mounting Systems: A Survey, ASME (2001).
[16] Bogdan Sapiński, Janusz Gołdasz, Development and performance evaluation of an MR squeeze-mode damper, Smart Materials and Structures 24(11) (2015).
[17] Abdul Yasser Abd Fatah, Saiful Amri Mazlan, Tsuyoshi Koga, et al., A review of design and modeling of magnetorheological valve, International Journal of Modern Physics B 29(04) (2015).
[18] D. H. Wang, H. X. Ai, W. H. Liao, A magnetorheological valve with both annular and radial fluid flow resistance gaps, Smart Materials and Structures 18(11) (2009).
[19] Alireza Farjoud, Ryan Cavey, Mehdi Ahmadian, et al., Magneto-rheological fluid behavior in squeeze mode, Smart Materials and Structures 18(9) (2009).
[20] Xuan Phu Do, Seung-Bok Choi, High Loaded Mounts for Vibration Control Using Magnetorheological Fluids: Review of Design Configuration, Shock and Vibration 2015 (2015) 1-18.
[21] Fitrian Imaduddin, Saiful Amri Mazlan, Mohd Azizi Abdul Rahman, et al., A high performance magnetorheological valve with a meandering flow path, Smart Materials and Structures 23(6) (2014).
[22] Do Xuan Phu, Kruti Shah, Seung-Bok Choi, A new magnetorheological mount featured by changeable damping gaps using a moved-plate valve structure, Smart Materials and Structures 23(12) (2014).
[23] Do Xuan Phu, Seung-Bok Choi, Vibration control of a ship engine system using high-load magnetorheological mounts associated with a new indirect fuzzy sliding mode controller, Smart Materials and Structures 24(2) (2015).
[24] Chulhee Han Soon-Yong Yang, Chul-Soo Shin and Seung-Bok Choi*, Dynamic characteristics of passive and semi-active cabin mounts for vibration control of a wheel loader, International Journal of Heavy Vehicle Systems 26(2) (2019) 239-261.
[25] Sung-Ryong Hong, Seung-Bok Choi, Vibration Control of a Structural System Using Magneto-Rheological Fluid Mount, Journal of Intelligent Material Systems and Structures 16(11-12) (2016) 931-936.
[26] Peng Chen, Xian-Xu Bai, Li-Jun Qian, et al., A magneto-rheological fluid mount featuring squeeze mode: analysis and testing, Smart Materials and Structures 25(5) (2016).
[27] Q. H. Nguyen, Seung Bok Choi, Y. S. Lee, et al., Optimal design of high damping force engine mount featuring MR valve structure with both annular and radial flow paths, Smart Materials and Structures 22(11) (2013).
[28] Shaoqi Li, Peter A. Watterson, Yancheng Li, et al., Improved magnetic circuit analysis of a laminated magnetorheological elastomer device featuring both permanent magnets and electromagnets, Smart Materials and Structures 29(8) (2020).
[29] Izyan Iryani Mohd Yazid, Saiful Amri Mazlan, Takehito Kikuchi, et al., Design of

magnetorheological damper with a combination of shear and squeeze modes, Materials & Design 54 (2014) 87-95.
[30] Izwan Ismail, Saiful A. Mazlan, Hairi Zamzuri, et al., Fluid–Particle Separation of Magnetorheological Fluid in Squeeze Mode, Japanese Journal of Applied Physics 51 (2012).
[31] Peng Chen, Xian-Xu Bai, Li-Jun Qian, Magnetorheological fluid behavior in high-frequency oscillatory squeeze mode: Experimental tests and modelling, Journal of Applied Physics 119(10) (2016).
[32] Xin-Jie Zhang, Alireza Farjoud, Mehdi Ahmadian, et al., Dynamic Testing and Modeling of an MR Squeeze Mount, Journal of Intelligent Material Systems and Structures 22(15) (2011) 1717-1728.
[33] Tao.R, Super-strong magnetorheological fluids, Journal Of Physics: Condensed Matter 13 (2001) 979-999.
[34] Yancheng Li, Jianchun Li, Weihua Li, et al., Development and characterization of a magnetorheological elastomer based adaptive seismic isolator, Smart Materials and Structures 22(3) (2013).
[35] Shaoqi Li, Yajun Liang, Yancheng Li, et al., Investigation of dynamic properties of isotropic and anisotropic magnetorheological elastomers with a hybrid magnet shear test rig, Smart Materials and Structures 29(11) (2020).